Uni-traveling-carrier photodiodes

Tadao Ishibashi and Hiroshi Ito

View Online   Export Citation   CrossMark

ARTICLES YOU MAY BE INTERESTED IN

Uni-traveling-carrier photodiodes

View Online   Export Citation   CrossMark

Tadao Ishibashi[1,a] 🆔 and Hiroshi Ito[2] 🆔

AFFILIATIONS

[1]NTT Electronics Techno Corporation, Morinosato-Wakamiya 3-1, Atsugi, Kanagawa 243–0198, Japan
[2]Center for Natural Sciences, Graduate School of Medical Sciences, Kitasato University, Sagamihara 252–0373, Japan

[a]**Email:** ishibashi-tadao@ntt-et.co.jp

ABSTRACT

The uni-traveling-carrier photodiode (UTC-PD) is a kind of pin junction photodiode that selectively uses electrons as active carriers. The diode structure has a relatively thin p-type absorber where electrons are generated as minority carriers, and then they diffuse and/or field-accelerate toward the collector. Since the electrons travel in the depleted collector at a ballistically high velocity, the photoresponse performance of a UTC-PD is superior to that of a conventional pin-PD. In this tutorial, the basics of the current response in a UTC-PD, the electron transport in the p-type absorber, and the performance of a terahertz-wave UTC photomixer, as a representative, are described.

I. INTRODUCTION

Any systems that handle high-speed optical signals commonly use junction-based photodiodes as detectors. At the photonic front end of communication systems, for example, the electrical postamplification of the photodetector output tends to limit the receiver performance in terms of frequency response and noise. Even in the existing highest speed fiber-optic transmission systems with a baud rate of several 10 gigabits per second, such a situation may not have been changed. Consequently, because the operation speed of optical receivers has been limited by electronic circuits, critical design optimization for a photodiode structure, typically of a pin-photodiode (pin-PD), has not been needed.

In a broader sense, however, an optical receiver can also be configured by replacing an electronic postamplifier with an optical preamplifier, provided that a photodiode has sufficient output linearity and dynamic range. Because a photodiode has no amplification process, it can potentially operate faster than a transistor circuit, and a photonic receiver using an optical amplifier has a broader bandwidth than that using an electronic one. In 1997, it was demonstrated that a newly designed photodiode, the uni-traveling-carrier photodiode (UTC-PD), could operate faster and with much wider output linearity simply by excluding the hole transport contribution to the diode operation.[1] Experimental results on a UTC-PD confirmed that the electron transport in the device is quasiballistic or in velocity overshoot when the bias voltage is kept in a low range.[1–3,14] The importance of such a nonequilibrium transport in a photodiode structure was first pointed out in these work, though similar structures had been reported before.[4–6]

Modification of the UTC-PD structure by combining depleted absorbers (hybrid absorber, dual absorber, partially depleted absorber, etc.) has also been reported.[7–15] This modification of hybrid absorbers is effective in terms of mitigating the trade-off relation between bandwidth and efficiency. In other words, the modified photodiode design can maximize efficiency for a certain required bandwidth, which has been discussed in detail in Ref. 14. One of the most valuable applications of UTC-PDs is photonic millimeter-wave and terahertz (THz)-wave generators known as "photomixers."[14,16] UTC-PDs have also been used in many applications including DQPSK receivers and integrated coherent receivers (ICRs) for improving sensitivity.[12,17] The concept of UTC design was also incorporated into avalanche photodiodes (APDs), which are now used in high-speed, high-sensitivity receivers.[18,19]

In this tutorial, we first clarify how the UTC-PD operates differently from the conventional pin-PD. The carrier transport in the p-type InGaAs absorber is then discussed in detail, since this is the key feature of the UTC operation. Monte Carlo simulations were performed to predict delay time in p-type InGaAs absorbers, where we focus on the use of a quasifield for electrons. As a case study, a THz-wave UTC photomixer is described, where we observe the frequency dependence of THz-wave radiation power reflecting the nonequilibrium feature of the electron transport.

II. PHOTORESPONSE COMPARISON OF PIN-PD AND UTC-PD

Both the pin-PD and UTC-PD are composed of heterostructure pn junction diodes. As illustrated in Fig. 1(a), the pin-PD has
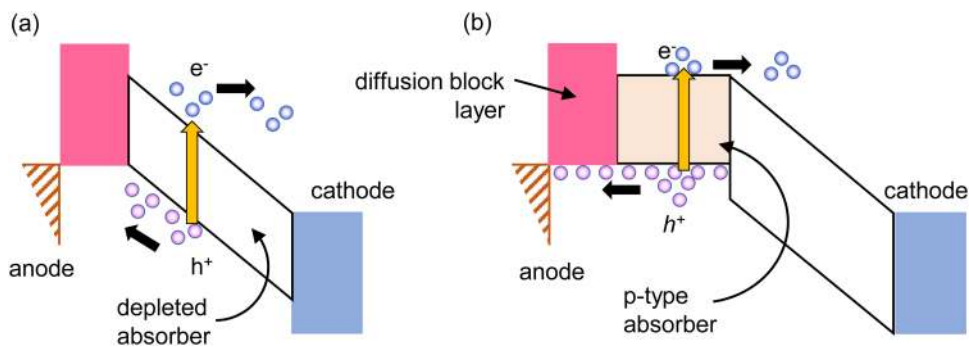
FIG. 1. Band diagrams of (a) pin-PD and (b) UTC-PD.

a depleted absorber sandwiched by wide-bandgap anode and cathode layers. The representative UTC-PD structure, Fig. 1(b), features a p-type neutral absorber and a wide-bandgap electron collection layer (collector), where a diffusion block layer on the anode side of the absorber provides photogenerated minority electrons with unidirectional flow to the collector. Background majority holes in the p-type absorber screen following the motion of electrons if the operation frequency of an incident optical signal is lower than the dielectric relaxation frequency depending on the hole concentration.[20] Also, the conduction photocurrent is uniform over the absorber maintaining charge neutrality and current continuity. In the pin-PD structure, photogenerated carriers are immediately accelerated in the depletion electric field and the averaged carrier traveling distance is half of the depletion layer. In the UTC-PD, in contrast, there is a delay time due to the minority electrons traversing over the p-type neutral absorber, and the traveling distance is just the depletion width. The key point here is that the mobility of the minority electrons in direct-gap III–V materials

(for example, InGaAs) is high and quasiballistic electron transport appears in the collector, so the total delay time associated with electron transport can be reasonably short.

Time domain on-wafer measurement gives more direct information of the photodiode behavior explained above, though the frequency domain technique generally gives better accuracy. To observe the pulse response of a photodiode, a pump-probe electro-optic sampling (EOS) technique can be used, where the electrical output signal profile is converted into an optical signal at the electro-optic crystal placed on the transmission line connected to a diode output port. Figures 2(a) and 2(b) show the EOS signals measured for an InP/InGaAs pin-PD and an InP/InGaAs UTC-PD, respectively, where the InGaAs depleted absorber thickness for the former and the InP collection layer thickness for the latter are made the same (300 nm). The diode junction areas are also the same ($20\,\mu m^2$) for the two diode structures. The input optical pulse intensity was changed from 0.2 to 2.0 pJ/pulse (FWHM was 400 fs), and the diode bias voltage was $V_{bias} = -2.0$ V.
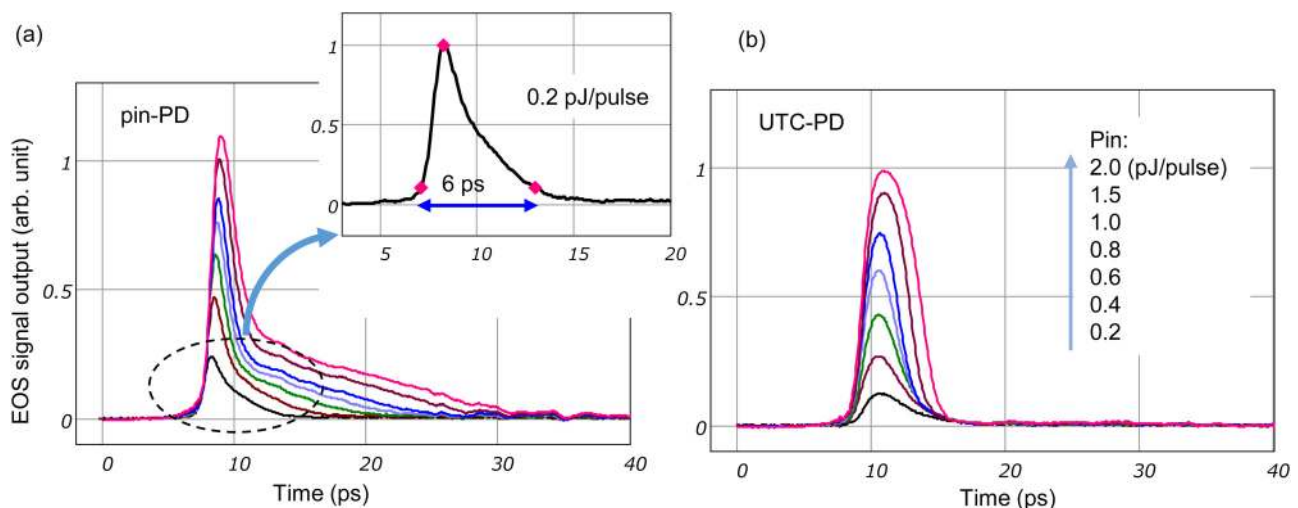

FIG. 2. Output signals observed by EOS measurement for (a) pin-PD and (b) UTC-PD. In the measurements, bias voltage and effective load resistance were −2.0 V and 25 Ω, respectively.

Since the two 50 Ω coplanar waveguide (CPW) lines are connected to the PD output on both sides of the device, the effective load resistance is 25 Ω and the corresponding RC time constant is ∼200 fs.

We found that the output signal profiles between a pin-PD and a UTC-PD are quite dissimilar. In the former, steep (by electron) and slower (by holes or holes + electrons) components are seen [Fig. 2(a)]. In this case, the linear response range in the pin-PD is for an input up to around ∼0.4 pJ/pulse. At higher input levels, the long tail part of the signal further extends, indicating a growing nonlinearity. When two kinds of conductions couple each other, the profile cannot be separated into two components in principle. In a linear response range, a slower long tail is resulting from the hole transport. Here, a signal full width as large as 6 ps at 0.2 pJ/pulse excitation leads to a calculated average carrier velocity of ∼5×10^6 cm/s, which is close to the hole saturation velocity in InGaAs. The small signal 3-dB down bandwidth (f_{3dB}) is, therefore, dominated by the response of the hole transport. The early sharp response of electrons does not influence the determination of f_{3dB}.

The change in the output photoresponse of the UTC-PD observed under the same input and bias conditions as the case of a pin-PD is shown in Fig. 2(b). The p-InGaAs thickness was designed to be 2200 A so as to have a similar small signal bandwidth f_{3dB} (90 GHz) as that of the pin-PD discussed above. In contrast to the pin-PD, the output signal of the UTC-PD exhibits no long tails. Moreover, the signal profile does not show any sharp increase compared to those we have seen in the pin-PD. This is due to the delay associated with electron diffusion in the p-InGaAs absorber, in which velocity by thermal motion is relatively slow. In addition, the electron traverse distance is doubled compared to a pin-PD. At optical input levels of up to around 1.0 pJ/W, no significant change in the output signal width is observed. The nonlinear behavior appears at the higher input levels simply as pulse broadening of output signals. This kind of output saturation is similar to the "Kirk effect" well known in bipolar transistors. It is also interesting to see that the signal fall time after the pulse broadening does not become large.

In general, the nonlinear effect originates from the space charge accumulation that modulates the field and potential profile of the depletion layer. Since holes do not participate in this phenomenon in a UTC-PD, the carrier transport there becomes much less complicated. A key point here is that an electron is much more mobile than a hole by a factor of 10 (due to ballistic velocity) to 20 (as mobility ratio), which makes the electron charge accumulation much weaker than the hole charge one. This is the basic reason for the better output linearity of the UTC-PD. From the power spectrum of a pulse signal, an effective number of f_{3dB} can be calculated even in the nonlinear output range. Such f_{3dB} of a pin-PD shows a significant decrease with increasing optical input due to the growing long tail portion. In contrast, UTC-PDs provide a much higher output without losing bandwidth.

III. TREATMENT OF CURRENT COMPONENTS IN A UTC-PD

Prior to a detailed discussion on electron transport in the p-type neutral absorber, we consider how the output is related to the electron and hole current components in a UTC-PD.

The minority electron flow, carrier distributions, and current components are schematically depicted in Fig. 3, where electron hole pairs are assumed to be excited by a sinusoidal generation rate $G_e(\omega)$ uniformly over the absorber with a thickness of W_{AN}. The flow of photogenerated minority electrons, which is blocked at the diffusion block layer on the anode side, produces a unidirectional current. The signal perturbation rate $1/\omega$ is usually slower than the dielectric relaxation time in a highly doped p-type absorber. In this case, the absorber photocurrent $J_{AN}(\omega)$, which is the sum of minority electron current $J_e(\omega)$ and background hole current $J_h(\omega)$,

$$J_{AN}(\omega) = J_e(\omega, x) + J_h(\omega, x) = -qG_e(\omega) \times R_{AN}(\omega), \quad (1)$$

is uniform over the absorber,[20] where $R_{AN}(\omega)$ is the frequency response of the absorber current determined by the minority electron transport. The electrons can flow even without a field, which gives a diffusive current that linearly increases with position x. Here, in order to have hole current $J_h(\omega, x)$ in Eq. (1), it needs a "self-induced field" for hole drift motion. The presence of this self-induced field was confirmed for uniformly doped p-type absorbers.[21] The electrons injected from the absorber edge propagate in the collector with velocity $v_e(x)$, and the total current is the sum of this conduction and displacement current,

$$J_{eColl}(\omega, x) = J_{AN}(\omega) \times \exp[j\omega(t - t'(x))] + \epsilon_S \frac{\partial E_C(\omega, x)}{\partial t}. \quad (2a)$$
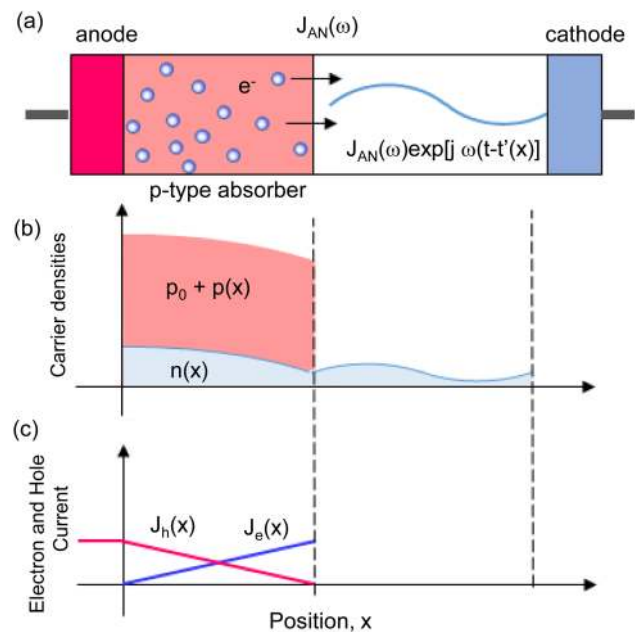

FIG. 3. Minority electron flow (a), carrier distributions (b), and current components (c).

Here, the delay time $t'(x)$ required for electrons to propagate to a position x is a function of $\nu_e(x)$ and given as

$$t'(x) = \int_0^x \nu_e(y)^{-1} dy. \tag{2b}$$

Diffusive motion of electrons during the propagation that reduces the current amplitude $J_{AN}(\omega)$ is not considered here. The collector current is then calculated by integrating $J_{eColl}(\omega,x)$ over the collector (W_C) as

$$J_{Coll}(\omega) = \frac{1}{W_{AN}} \int_0^{W_C} J_{eColl}(\omega, x) dx = J_{AN}(\omega) R_{Coll}(\omega) + \epsilon_S \frac{1}{W_C} \frac{\partial V_C(\omega)}{\partial t}, \tag{3}$$

where $R_{Coll}(\omega)$ is the frequency response of the collector conduction current, and $V_C(\omega)$ is the voltage drop over the collector. Because the amplitude and phase differ between injection current $J_{AN}(\omega)$ and collector conduction current $J_{AN}(\omega) R_{Coll}(\omega) = J_C(\omega)$, an additional current term $J_{adj}(\omega)$, which was missing in earlier treatment,[1] must be present in order to satisfy the current continuity, as

$$\begin{aligned} J_{tot}(\omega) &= J_{AN}(\omega) + \frac{j\omega\epsilon_s}{W_{AN}} V_{AN}(\omega) + J_{adj}(\omega) \\ &= J_C(\omega) + \frac{j\omega\epsilon_s}{W_C} V_C(\omega), \end{aligned} \tag{4}$$

assuming $V_{AN}(\omega)$ is the voltage drop in the absorber layer. The amplitude of $J_C(\omega)$ is smaller than that of $J_{AN}(\omega)$, and $J_{adj}(\omega)$ flows oppositely to $J_{AN}(\omega)$. At the same time, this $J_{adj}(\omega)$ partially induces $V_{AN}(\omega)$. To ensure zero terminal voltage in a short circuit condition, it must hold the balancing

$$\frac{j\omega\epsilon_s}{W_{AN}} V_{AN}(\omega) = -\frac{j\omega\epsilon_s}{W_C} V_C(\omega). \tag{5}$$

This means that $V_C(\omega)$ depends on $V_{AN}(\omega)$, which is determined by $J_{AN}(\omega)$, $J_{adj}(\omega)$, and absorber resistance R_A. Then, the output is modulated through the term $j\omega\epsilon_s(W_C^{-1}) V_C(\omega)$ in Eq. (4). At the low frequency limit, $J_{AN}(\omega)$ is equal to $J_C(\omega)$. This situation is mostly established in a high-speed UTC-PD operating at frequency $< f_{3dB}$; then, the adjustment current is approximated as

$$J_{adj}(\omega) = -2\frac{j\omega\epsilon_s}{W_{AN}} V_{AN}(\omega). \tag{6}$$

Assuming $|J_{AN}(\omega)| \gg |J_{adj}(\omega)|$ under a condition of sufficiently small R_A, Eq. (6) is deduced to

$$J_{adj}(\omega) \approx -2\frac{j\omega\epsilon_s}{W_{AN}} J_{AN}(\omega) \frac{R_{AN}}{2} = -j\omega C_{AN} R_A J_{AN}(\omega) = -j\omega\tau_{adj} J_{AN}(\omega). \tag{7}$$

The adjustment current time constant τ_{adj} is as short as several 10 fs; for example, in a p-InGaAs absorber with $R_A = 2.6 \times 10^{-7} \, \Omega \, cm^2$ estimated for $W_{AN} = 100 \, nm$ and $p = 10^{18}/cm^3$.

In this case, the $\omega\tau_{adj}$ value becomes >1 for a frequency higher than $\sim$1.5 THz.

Consequently, for a UTC-PD with a low resistive p-type absorber, the response deterioration associated with collector displacement current $-(j\omega\epsilon_s/W_C)V_C(\omega)$ can be ignored, and the response is approximated simply to $J_{AN}(\omega)R_{Coll}(\omega)$ as

$$J_C(\omega) \approx J_{AN}(\omega)R_{Coll}(\omega) = -qG_e(\omega) \times R_{AN}(\omega)R_{Coll}(\omega). \tag{8}$$

Of course, to suppress the influence by $-(j\omega\epsilon_s/W_C)V_C(\omega)$, the absorber may be thinner, more heavily doped, and/or graded doped without reducing the thickness W_{AN}.

IV. ELECTRON TRANSPORT IN A UTC-PD

A. Monte Carlo simulation

In the equilibrium (or steady state) condition, the photoresponse of a small-scaled diode can behave differently from that predicted by a drift-diffusive model where the carrier mobility μ_e, diffusivity D_e, and carrier velocity ν_e are treated as local parameters. In an actual high-speed photodiode, electron transport can be far from the equilibrium condition, and thus, "carrier saturation velocity," ν_s, at a high field has little meaning. In this section, we focus on nonequilibrium electron transport in a UTC-PD.

To investigate the electron dynamics in a UTC structure, we utilize Monte Carlo simulation. Here, the electron state is determined by repeating scattering and acceleration during a free flight time τ_{ff} as

$$\delta k_e(h/2\pi) = -qF\tau_{ff}, \tag{9}$$

where k_e is the wavevector of the electron state. In this calculation, each τ_{ff} is obtained from the exponential probability distribution function under a given total scattering rate and quasirandom number. After the acceleration, electron velocity is then calculated as group velocity for new k_e,

$$\nu_e(k_e, t) = (2\pi/h)dE_k/dk_e, \tag{10}$$

taking the band nonparabolicity into account. The scattering mode and scattering angle are also determined by using second and third random numbers. In this calculation, electron scattering mechanisms of only the LO-phonon, acceptors, and heavy holes are incorporated. Hole plasmon (HP) scattering was not taken into account due to its low scattering rate. The reason for the low scattering event is its smaller HP wavevector compared to Debye wave number and low HP energy. For simplicity, heavy holes are treated just like screened donors. We compared the simulated low field mobility values to reported results modeled by incorporating polar optical phonon–plasmon coupling[22] and found that the present calculation still has a similar variation with the acceptor doping level for a doping range of up to the middle of $10^{18}/cm^3$ (Fig. 4).

B. Carrier excitation, relaxation, and acceleration

When minority electrons flow diffusively in a p-type neutral absorber, the carrier temperature, or their average energy, is important. Depending on their initial energy distribution, electrons can
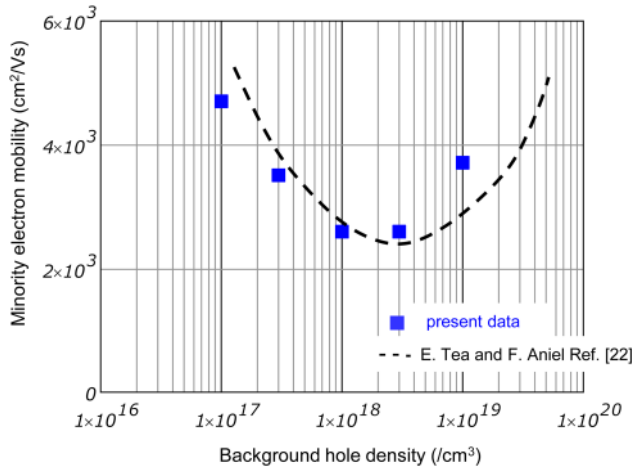
FIG. 4. Comparison of simulated minority electron mobility in p-InGaAs.

transiently become hot or cool both relaxing to equilibrium energy. Moreover, how the initial condition influences the total delay time will vary with the absorber structure. Pulse photoresponse is used because simulating it takes less time than simulating the continuous wave (RF) response. When electrons are excited by absorbing the incident photons, the momentum conservation is not conditioned, since the absorber dimension and electron mean free path are shorter than the excitation wavelength. The probability $P_{exc}(E_e, E_{exc})$ for electrons positioned at energy E_e is assumed to be proportional to the coupled density of states,

$$P_{exc}(E_e, E_{exc}) = C_1[E_e(E_{exc} - E_G) - E_e^2], \quad (11)$$

where E_G, E_{exc}, and C_1 are the bandgap energy, optical excitation energy, and a constant, respectively. After determining the electron energy, the wavevector of the electron is randomly distributed.

First, we examine the behavior of minority electrons in a p-InGaAs when they are optically excited in a space without structure (no boundary conditions). Figure 5 shows the simulated temporal changes in the average energy of electrons $\langle E_e(t)\rangle$ in uniformly doped p-InGaAs $(1 \times 10^{18}/\text{cm}^3)$ excited at 1300-nm, 1550-nm, and 1625-nm wavelengths. The energy relaxations happen over time (0.5–1 ps) so that the systems will settle to those in the equilibrium level $(1.5k_BT)$. In the case of 1300-nm excitation, the electron energy distributes initially from 0 to 200 meV with a mean energy of 100 meV. In a period of 1 ps, an electron experiences roughly twice as many phonon absorptions and six times as many emissions in probability. Thus, the net cooling rate is equivalent to four times the LO phonon energy $4 \times (h/2\pi)\omega_{LO} = 132$ meV, which is comparable to the initial mean energy. This is the reason for the relatively slow cooling process. Just after the excitation, the diffusion motion of these "hot" electrons can become faster than that in equilibrium. Therefore, the excitation wavelength should be considered when optimizing the UTC structures.

Figure 6 plots the group velocity $v_e(k)$ of electrons 200 fs after the 1550 nm excitation in a structure with a p-InGaAs layer $(W_{AN} = 100$ nm, $p = 1 \times 10^{18}/\text{cm}^3)$ and depleted collector $(W_D = 200$ nm). The blue dot shows individual electron group velocity $v_e(k)$ simulated for 20 000 particles. In the present simulation, Γ to satellite valley transition is not considered here because Γ- to L-valley separation energy is as high as 800 meV. The average electron velocity $\langle v_e(k)\rangle$ in a spatial partition of 5 nm is also shown. The collector is assumed to be made of InGaAs for simplicity with its field intensity of 30 kV/cm. At 200 fs after photoexcitation, electrons mostly remain in the p-InGaAs absorber with random velocity directions. At the same time, some electrons are found to be ballistically driven by field and some particles are already close to the anode layer, though the averaged group velocity increases more slowly. This simulation example indicates that the traveling velocity in the collector is very high and the absorber traveling time tends to dominate the total delay time in a UTC-PD structure. The saturation tendency of the ballistic velocity occurs due to reduced acceleration originating from the band nonparabolicity. When a high diode bias voltage is applied, Γ to satellite valley transition reduces
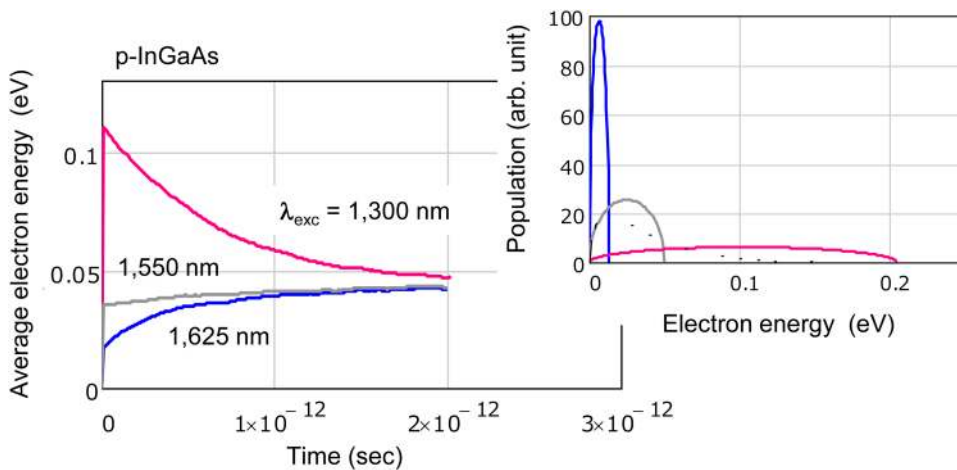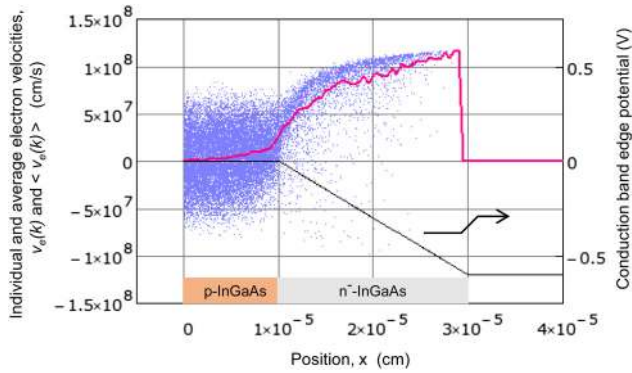

FIG. 5. Variation of average electron energy excited at 1300, 1550, and 1625 nm wavelengths. Energy distributions at the initial conditions are also shown on the right.

FIG. 6. Plot of individual electron velocity $v_e(k)$ (blue dots) and average electron velocity $\langle v_e(k) \rangle$ (red line).

electron velocity, showing a velocity overshoot.[23] Therefore, small bias voltage is essentially important in maintaining fast response in a UTC-PD structure.

In Eq. (2a) before, we assumed that electrons propagate in the collector ignoring their diffusive motion. It is found in Fig. 6 that individual $v_e(k)$ distributes very widely and the condition of "no-diffusion" seems to be broken. However, the curve of averaged one $\langle v_e(k) \rangle$ is close to the ballistic line, and thus, such assumption can be used. At the absorber-collector layer boundary, simulated $\langle v_e(k) \rangle$ is 2.6×10^7 cm/s that coincides with twice the value (= value for the hemi-Maxwellian) of the thermionic emission velocity, $v_{th} = (k_B T / 2 m_e^* \pi)^{1/2}$. Although $\langle v_e(k) \rangle$ is high at the boundary, it is quite low in the p-InGaAs layer compared to that in the collector.

C. Incorporation of quasifield by graded doping

We next examine how the velocity profiles and absorber delay times differ among uniform doping and graded doping structures. An InP/InGaAs UTC-PD performs better when it incorporates a quasifield in the p-type absorber tailored by a graded doping as illustrated in Fig. 7(a). When the doping level changes with depth, a quasifield F_{quasi} that accelerates minority electrons can be generated, though the majority holes do not benefit from it due to their backward diffusion motion. Change in background doping by one decade can induce about 60 meV (6 kV/cm over 100 nm) at room temperature. Since the minority electron mobility is high (e.g., $\mu_e = 2600$ cm²/V s at $p = 1 \times 10^{18}$/cm³), the drift velocity $v_d = \mu_e F_{quasi}$ can be effectively high. In the modeled quasifield structure, the doping level was exponentially graded over W_{AN} changing from 2×10^{17}/cm³ (collector side) to 6×10^{18}/cm³ (anode side). Taking the bandgap shrinkage dependence on the doping level into account, F_{quasi} was calculated as 7.3 kV/cm at the collector end and decreased to 3.9 kV/cm at the anode end. Figure 7(b) shows the velocity profiles of two kinds of structure at $t = 200$ fs after the carrier excitation, where the velocity profiles in the absorbers are already in the stationary state regardless of the number of remaining electrons. First, at the absorber-collector boundary, values of $\langle v_e(k) \rangle$ are 2.6×10^7 and 4.1×10^7 cm/s for the uniformly doped and quasifield structures, respectively. Inside
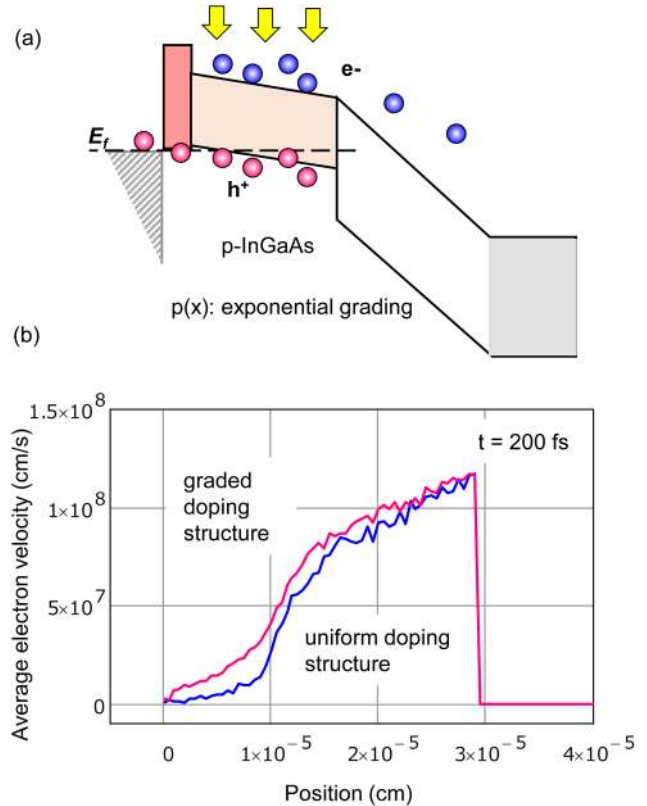
FIG. 7. InP/InGaAs UTC-PD incorporating a quasifield (graded doping) in the p-type absorber (a) and velocity profiles for two kinds of structures at $t = 200$ fs after carrier excitation (b).

the absorber, more importantly, a significant difference in $\langle v_e(k) \rangle$ exists. This is the reason for much faster photoresponse realized in a graded doping structure. We also see that the velocity decreases considerably toward the anode. The question is, then, how does the quasifield accelerate the electrons? The minority electron mobility μ_e simulated by using the same scattering rates is as high as 2600 cm²/V s for $p = 1 \times 10^{18}$/cm³. Simply estimating a drift velocity, $v_{de} = \mu_e F_{quasi}$ is deduced to 1.9×10^7 cm/s. This value, $\mu_e F_{quasi} < 2 v_{th}$, means that the diffusion mechanism still helps electrons to be swept to the collector. The momentum relaxation time τ_m evaluated by μ_e is 62 fs. Without diffusive motions, the electron drift velocity increases with a time constant τ_m and saturates at v_{de}. The electron velocity profiles shown in Fig. 7 are at a time 200 fs after excitation, and thus, they are in stationary condition. Consequently, low electron drift velocity on the anode side $<\mu_e F_{quasi}$ is found to be resulting from diffusive current component flowing in the reverse direction to that of photoresponse current.

V. ABSORBER DELAY TIME

In evaluating the photoresponse speed of electron motion in a p-type absorber, we introduce the absorber delay time τ_A. The total electron charge in the absorber Q_A is assumed to change with a

time constant τ_A as

$$\frac{dQ_A}{dt} = -Q_A/\tau_A + qG_e(t),\qquad(12)$$

where $G_e(t)$ is the carrier generation rate. For the pulse response with $G_e(t) = 0$ at $t > 0$, the charge variation $q^{-1}dQ_A/dt$ is equal to the rate of electron flow to the collector. While this assumption may seem simple, it well approximates the response for a case when $J_{AN}(t)$ has a similar phase with that of Q_A.[24] Furthermore, this case provides a frequency response for a carrier generation of G_{eRF},

$$J_{AN}(\omega) = -qG_{eRF}R_{AN}(\omega) = -qG_{eRF}(1 + j\omega\tau_A)^{-1}.\qquad(13)$$

To suppress the noise associated with the number of particles in Monte Carlo simulation, it is better to use pulse response, where Q_A can change with time having a simple form as

$$Q_A(t) = Q_{A(t=0)}\exp\left(-\frac{t}{\tau_A}\right).\qquad(14)$$

If a simulated charge variation fits an exponential time dependence, it indicates that the photocurrent response was well approximated by Eqs. (12) and (13). In fact, the good fitting conditions were achieved. Figure 8(a) shows the variation of τ_A with p-InGaAs thickness W_{AN} obtained by fitting an exponential curve to the simulated Q_A variations by Eq. (14). Here, two kinds of p-type absorber structures, uniform doping and graded doping (quasifield structure), are investigated. We found that the graded doping structure has a considerably smaller τ_A than the uniform doping structure by a factor of 2–4 in the calculated W_{AN} range. At $W_{AN} = 100$ nm, for example, the graded doping structure gives $\tau_A = 0.39$ ps, which is 37% that of a uniform doping structure. Because the quasifield structures have steeper τ_A vs W_{AN} variation,

the benefit of the quasifield structure is more pronounced in a smaller W_{AN}. This advantage in τ_A directly reflects on the responsivity. Namely, for requested bandwidth, the responsivity can be largely improved.

What is happening in the uniformly doped structure? If the delay time is dominated by the simple diffusive process with local diffusion velocity $v_e(x) \ll v_{th}$, τ_A should be proportional to W_{AN}^2, while the τ_A curve obtained by simulation varies, which is proportional to $W_{AN}^{1.3}$. On the other hand, at the "no scattering" limit, τ_A is given by $W_{AN}/2v_{th}$, because half of the electrons excited in the absorber traverse with velocity $2v_{th}$ and the other half with $-2v_{th}$. Therefore, in the W_A range simulated here, the electron transport is not of simple diffusion; rather, they tend to be swept to the collector maintaining their initial velocity vectors.

Let us take a closer look at the assumption expressed in Eq. (12). At $t = 0$, all electrons start to change their position, momentum, and energy in the given environment. Therefore, this environment naturally has transient characteristics due to the field. It is found that Q_A variation of the graded doping structure has a certain delay time Δt_{acc} when migrating into exponential change [Fig. 8(c)]. Similar type of delay is not seen in the uniform doping structure [Fig. 8(b)]. For $W_A = 100$ nm shown in Fig. 8(c), Δt_{acc} concerning this "initial acceleration" is estimated to be ~50 fs, which is close to the momentum relaxation time τ_m calculated for a mobility value of $\mu_e = 2600$ cm^2/V s. As a result of this transient feature, the corresponding power spectra intensity is less in the high frequency range than that without Δt_{acc}.

VI. CASE STUDY: TERAHERTZ-WAVE UTC PHOTOMIXER

UTC-PDs and their derivative structures have been used as terahertz-wave generators. The UTC-PD chip is packaged in a rectangular-waveguide module or both the UTC-PD and a planar
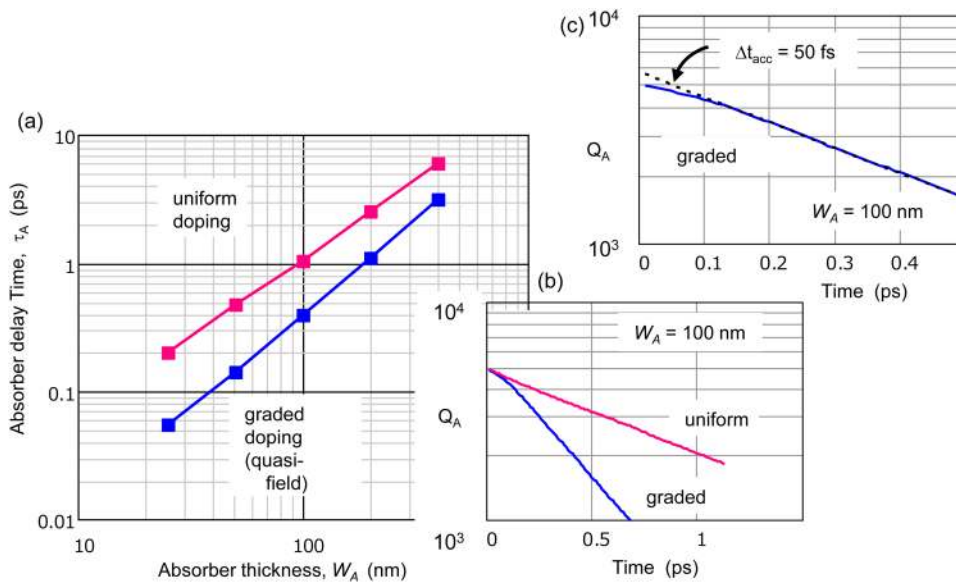
FIG. 8. Simulated absorber delay time for InP/InGaAs UTC-PDs with uniform doping and graded doping (a). Comparison of the change in absorber charge Q_A is shown in (b). There is a small delay in a graded doping structure (c).

antenna are integrated on the same InP substrates. By OE conversion of an optical two-mode beat signal to a photodiode current, terahertz-wave (THz-wave) radiation is easily generated. Since the optical beat consists of superimposed fields $(E_1 + E_2)$ by λ_1 and λ_2 modes, the photon energy absorption rate, which is proportional to $(E_1 + E_2)^2$, has a beat envelope. Though the OE conversion happening here in the photodiode is the linear process, this type of operation is called "photomixing," from an analogy of electron devices.

As discussed in Sec. II, a significant advantage of introducing the UTC design is improvement in the possible output in a THz frequency range where electronic amplification is not available. To date, continuous wave radiation at frequencies higher than 5 THz has been reported.[25]

Figure 9 is a schematic band diagram of a UTC-PD with a modified absorber. The p-type absorber (thickness of W_{AN}) features graded doping to yield an effective quasifield and the depleted absorber is placed with a thickness W_{AD} adjusted to 1/4 to 1/2 of the total collector depletion thickness W_{Coll}. At a required total absorber thickness $W_A = W_{AN} + W_{AD}$, and a fixed W_{Coll}, there exists the best set of partition for W_{AN} and W_{AN} maximizing the bandwidth f_{3dB}. Because f_{3dB} determined in such a way is a monotonic function of W_A, any best set simultaneously presents the highest responsivity (maximum W_A) at a fixed f_{3dB}. A detailed discussion was given in Ref. 14. An induced current amplitude originating from holes is not proportional to W_{AD} because it is a quantity integrated over a range of W_{Coll}. For a given W_{AD}, the intensities of hole- and electron-induced current components are proportional to $W_{AD}/2$ and $W_{AD}/2 + (W_{Coll} - W_{AD})$, respectively, in a low frequency limit. When the W_A/W_{Coll} ratio is 1/4 to 1/2, the hole current intensity produces 1/7 to 1/3 that of the electron current one (−17 dB to −10 dB in power), which is sufficiently low for photomixer operation. Of course, since there is also an electron current component that originates from the neutral absorber, the contribution of the hole current is even smaller.

A bowtie antenna-integrated UTC photomixer chip and quasioptic module with fiber pigtail are shown in Fig. 10. The fabricated UTC structure grown on an InP substrate by MO-VPE has a p-type InGaAs absorption layer ($W_{AN} = 300$ A) with graded doping
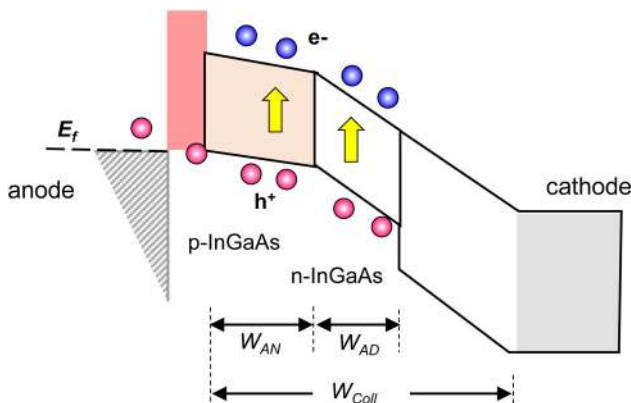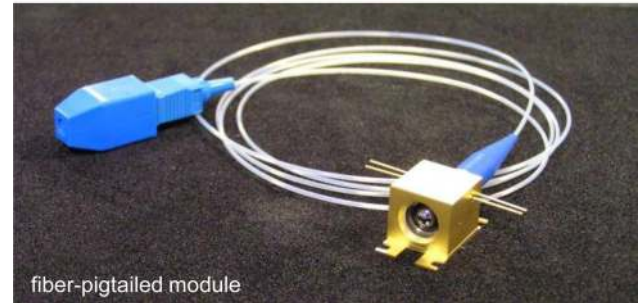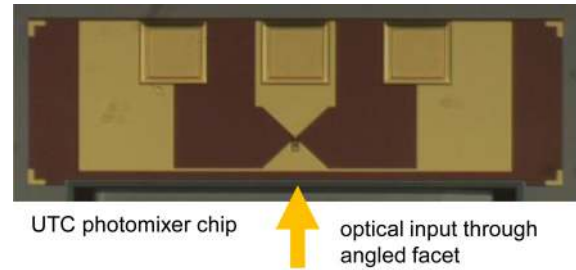

FIG. 10. A bowtie antenna-integrated UTC photomixer chip and quasioptic module with a fiber pigtail.

and a depleted absorption layer ($W_{AD} = 1000$ A).[14] The depletion layer is 0.23 μm thick and consists of a depleted InGaAs absorber, a thin InGaAsP interlayer, and an InP electron traveling layer. The junction area is $\sim 20\,\mu m^2$ defined by wet mesa etching. The UTC-PD chip, 1×0.5 mm^2 in size, is placed on a hyper hemispherical Si lens (5-mm diameter). The THz-wave radiation is emitted from the antenna through a Si lens where the effective load impedance of the diode is $\sim 75\,\Omega$, as calculated for a planar bowtie antenna on an InP substrate.[26] The typical frequency dependence of THz output power of the fabricated UTC photomixer is shown in Fig. 11, where the operation photocurrent is 6 mA and the bias voltage is −0.4 V (collector field $F_{Coll} = 40$ kV/cm). The observed radiation output (blue square) changes gradually with a frequency of up to around 3 THz. The solid lines indicate the calculated output variation, where we assumed an absorber delay time τ_A of 43 fs and average electron velocity in the collector v_{eColl} changing from 1×10^7 to 1×10^8 cm/s as a parameter. Because THz propagation loss is not excluded here, the plot of the experimental data lies on the 5–6-dB lower level. It is obvious here that the assumed v_{eColl} as saturation velocity never explains the experimental result, and the quasiballistic electron transport, 6×10^7 to 1×10^8 cm/s, must exist in the collector. Leitenstorfer et al. investigated electron velocity overshoot in an InP pin diode by femtosecond optical excitation[27] and found the velocity to be around 6×10^7 cm/s at a field of 50 kV/cm. The observed v_{eColl} in both experiments is consistent.

One problem is the RC time constant. For example, while the calculated intrinsic 3-dB down bandwidth f_{3dB} is as high as 900 GHz for the v_{eColl} of 6×10^7, the RC time constant is calculated to be 75 $\Omega \times$ 11.3 fF = 850 fs, which yields a bandwidth of f_{3dB}(RC) = 190 GHz, significantly reducing the overall 3-dB down

FIG. 9. Band diagram of a UTC-PD with modified absorber.
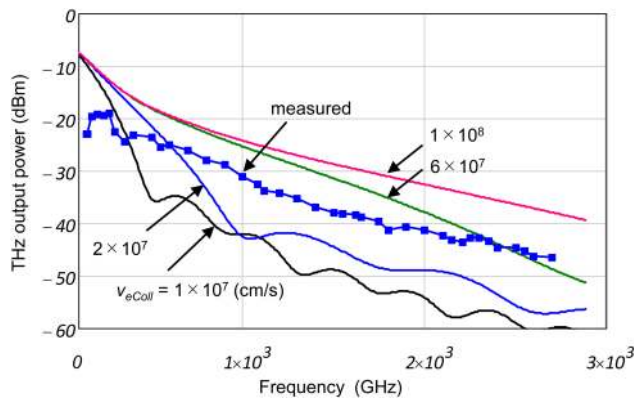
FIG. 11. Frequency dependence of THz-wave photomixer output power and the calculated variations when changing the effective electron velocity v_{eColl} as a parameter.

bandwidth in actual devices. Note that f_{3dB} values on calculated curves do not differ largely for $v_{eColl} = 2 \times 10^7$, 6×10^7, and 1×10^8 cm/s. In the higher frequency range of $f > 500$ GHz, however, the calculations predict a dramatic change in output depending on v_{eColl}, which is simply because the intrinsic response possesses a steeper frequency dependence than RC time constant.

Diode bias dependence of the photomixer output also provides information on the carrier transport in the UTC structure.[14] Figure 12 shows the variation of measured THz output with bias V_{bias} at fixed frequencies of $f = 250$, 500, 1000, and 1700 GHz. We found there is an optimum bias voltage $V_{bias}(\text{opt})$. The lower output at a bias smaller than $V_{bias}(\text{opt})$ is due mostly to a smaller response given by the lower electron velocity. At the same time, the output decreases at the higher V_{bias}, and this is more pronounced at higher frequencies. Here, the output linearity is confirmed for the bias at least >0 V and the photocurrent condition of 6 mA. The diode junction capacitance is mostly constant, and the depletion
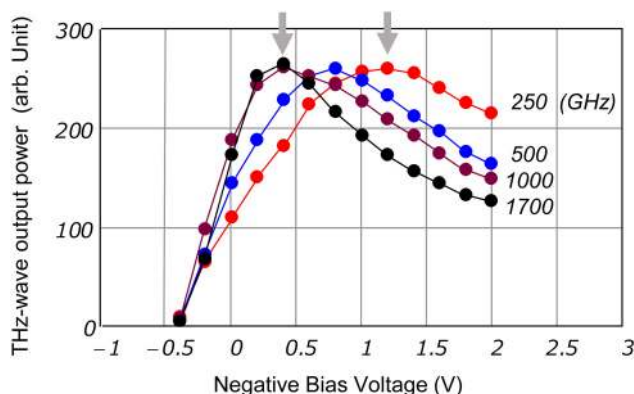
FIG. 12. Variation of measured THz output with bias V_{bias} at fixed frequencies of $f = 250$, 500, 1000, and 1700 GHz. The operation current is $I_{ph} = 6$ mA.

thickness is unchanged. The observed variation is, thus, dominated by the variation of electron velocity. To explain the change in output of 3 dB down at 1700 GHz, for example, there must be a velocity change from 1×10^8 cm/s to 6.5×10^7 cm/s calculated by the same model described above. With increasing frequency, the optimum V_{bias} point shifts from −1.5 V ($F_{Coll} = 78$ kV/cm) to −0.4 V ($F_{Coll} = 40$ kV/cm). How can we explain this shift of the optimum V_{bias}? While there is no easy answer, one probable reason is the change in the role of the hole current. The f_{3dB} of the hole current originating from the depleted InGaAs is around 200 GHz, assuming an effective v_h of 5×10^6 cm/s, so a small change in output with higher v_h at a larger bias can occur. The linearity in the diode operation is confirmed, so we know the output saturation mechanism is not at play here. Therefore, a possible shift of optimum bias to the reverse side for achieving a larger output swing cannot be a reason.

VII. SUMMARY AND FUTURE ISSUES

UTC design is simply the selective use of electron transport in a photodiode. In a pin-PD, we clearly observe a comparatively slow hole transport, unlike the electron transport. Electrons can be accelerated ballistically and their response is fast even in a pin-PD, but 3-dB down bandwidth (f_{3dB}) is determined by the hole response. The solution is a UTC design that incorporates a p-type absorber and/or an additional thin depleted absorber on the anode side. Furthermore, due to the high electron velocity, the field modulation by the space charge is much less in a UTC-PD. This is why a UTC-PD can provide a significantly higher output saturation level than a conventional pin-PD.

Electron transport in a UTC structure is far from that described by the conventional drift-diffusion picture using local parameters. This is because the electron system shows transient behavior that differs from those in equilibrium or steady state in a larger dimension. In evaluating the absorber delay time, Monte Carlo simulation has been employed in the present work. It has been found that the pulse photoresponse is well approximated by the exponential decay with a time constant that is the absorber delay time τ_A. The graded doping structure for a p-type absorber has been shown to provide significantly shorter τ_A than a uniform doping structure. In the graded doping structures, at the same time, both the drift and diffusive motions of electrons participate in determining the delays.

In the THz frequency range where a compact electronic amplifier is absent, an optical amplifier can replace it. Compared to the traditional electrical up-convertors, UTC photomixers can generate THz-wave radiation much easily using an optically amplified two-mode beat signal. When the optical beat is modulated electrically with data signals, THz radiation with data can be directly obtained through the OE conversion.

As we have seen, however, the output level in the THz frequency range is not necessarily high enough for certain applications. Therefore, we need technological improvements in device fabrication that can produce a higher output. Up to now, optimizations of the diode epitaxial layer and the matching circuit have been made. For further improvement, the heat dissipation capability is primarily important as microwave power transistor

technologies have experienced. Use of an intentional heat sink with a metal and/or heterogeneous substrate featuring higher thermal conductivity is desirable, where the signal propagation pass or waveguide-based coupling for the incoming optical beam can be maintained.

The power-combining technique, which is often utilized in electronic circuits, is known to be effective. Since THz-wave propagation loss on the transmission lines is rather high, there exists a limitation when it comes to combining the number of elements depending on frequency. When the output port is radiation medium, arrayed antennas can be used as a power combiner. Here, the transmission line from the photodiode to the antenna must be short enough. Besides, to enable beam forming functions, the signal at each antenna output must be phase controlled. To meet these requirements, we need a chip that integrates arrayed photodiodes located close to the antenna and allayed THz phase control devices. Consequently, for improving the THz-wave performance of UTC-PDs and developing their related applications, we need to gather together various technologies.

ACKNOWLEDGMENTS

REFERENCES

[1]T. Ishibashi, N. Shimizu, S. Kodama, H. Ito, T. Nagatsuma, and T. Furuta, *OSA TOPS on Ultrafast Electronics Optoelectronics* (OSA, 1997), Vol. 13, p. 83.

[2]H. Ito, T. Furuta, S. Kodama, and T. Ishibashi, Electron. Lett. **36**, 1809 (2000).

[3]H. Ito, S. Kodama, Y. Muramoto, T. Furuta, T. Nagatsuma, and T. Ishibashi, IEEE J. Sel. Top. Quantum Electron. **10**, 709 (2004).

[4]T. Pearsal, M. Piskorski, A. Brochet, and J. Chevrier, IEEE Quantum Electron. **17**, 255 (1981).

[5]F. J. Effenberger and A. M. Joshi, IEEE J. Lightwave Technol. **14**, 1859 (1996).

[6]G. A. Davis, R. E. Weiss, R. A. LaRue, K. J. Williams, and R. D. Esman, IEEE Photonics Technol. Lett. **8**, 1373 (1996).

[7]Y. Muramoto and T. Ishibashi, Electron. Lett. **39**, 1749 (2003).

[8]X. Li, S. Demiguel, N. Li, J. C. Campbell, D. L. Tulchinsky, and K. J. Williams, Electron. Lett. **39**, 1466 (2003).

[9]J.-W. Shi, Y.-S. Wu, C.-Y. Wu, P.-H. Chiu, and C.-C. Hong, IEEE Photonics Technol. Lett. **17**, 1929 (2005).

[10]A. Wakatsuki, T. Furuta, Y. Muramoto, T. Yoshimatsu, and H. Ito, *33rd International Conference on IRMMW-THz 2008* (IEEE, 2008), p. 1.

[11]A. Dyson, I. D. Henning, and M. J. Adams, IEEE J. Sel. Top. Quantum Electron. **14**, 277 (2008).

[12]T. Yoshimatsu, Y. Muramoto, S. Kodama, T. Furuta, N. Shigekawa, H. Yokoyama, and T. Ishibashi, Electron. Lett. **46**, 941 (2010).

[13]E. Rouvalis, C. C. Renaud, D. G. Moodie, M. J. Robertson, and A. J. Seeds, Opt. Express **18**, 11105 (2010).

[14]T. Ishibashi, Y. Muramoto, T. Yoshimatsu, and H. Ito, IEEE J. Sel. Top. Quantum Electron. **20**, 3804210 (2014).

[15]G. Zhou, P. Runge, S. Keyvaninia, S. Seifert, W. Ebert, S. Mutschall, A. Seeger, Q. Li, and A. Beling, IEEE J. Lightwave Technol. **35**, 717 (2017).

[16]H. Ito, T. Furuta, F. Nakajima, K. Yoshino, and T. Ishibashi, IEEE J. Lightwave. Technol. **23**, 4016 (2005).

[17]K. Murata, T. Saida, K. Sano, I. Ogawa, H. Fukuyama, R. Kasahara, Y. Muramoto, H. Nosaka, S. Tsunashima, T. Mizuno, H. Tanobe, K. Hattori, T. Yoshimatsu, H. Kawakami, and E. Yoshida, Opt. Express **19**, B125 (2011).

[18]M. Nada, H. Yokoyama, Y. Muramoto, T. Ishibashi, and H. Matsuzaki, Opt. Express **22**, 14681 (2014).

[19]M. Nada, Y. Yamada, and H. Matsuzaki, IEEE J. Sel. Top. Quantum Electron. **24**, 3800811 (2018).

[20]T. Ishibashi, S. Kodama, N. Shimizu, and T. Furuta, Jpn. J. Appl. Phys. **36**, 6263 (1997).

[21]N. Shimizu, N. Watanabe, T. Furuta, and T. Ishibashi, Jpn. J. Appl. Phys. **37**, 1424 (1998).

[22]E. Tea and F. Aniel, J. Appl. Phys. **109**, 033716 (2011).

[23]T. Ishibashi, IEEE Trans. Electron Devices **48**, 2595 (2001).

[24]T. Ishibashi, T. Furuta, H. Fushimi, and H. Ito, Proc. SPIE **4283**, 469 (2001).

[25]D. Fukuoka, K. Muro, and K. Noda, Proc. SPIE **9747**, 974717 (2019).

[26]S. S. Gearhart, J. Hesler, W. L. Bishop, T. W. Crowe, and G. M. Rebeiz, IEEE Microw. Guid. Wave Lett. **3**, 205 (1993).

[27]A. Leitenstorfer, S. Hunsche, J. Shah, M. C. Nuss, and W. H. Knox, Phys. Rev. Lett. **82**, 5140 (1999).